Electrostatic Patterns on Surfactant Coatings Change with Ambient Humidity

Juliana Silva Bernardes, Camila Alves Rezende, and Fernando Galembeck*

Institute of Chemistry, University of Campinas—UNICAMP, P.O. Box 6154, 13084-971, Campinas-SP, Brazil

Received: August 3, 2010; Revised Manuscript Received: October 5, 2010

Sodium dodecyl sulfate (SDS) deposited by dewetting on mica under well-defined experimental conditions presents patterns with characteristic morphology and electric potential distribution. These are formed by surfactant steps and terraces, with more negative potential on the steps than on the terrace surfaces. Kelvin force microscopy results show that the electric potential on the sample surfaces becomes more negative just by increasing the atmospheric relative humidity from 30 to 70%, within a grounded and shielded environment. The kinetic effect of the potential variation was also evaluated by keeping the sample at the same humidity for short (2 h) and longer times (24 h). In the last case, the electric potentials changed to more negative values, nonreversibly. Changes on the surface electric patterns are not paralleled by morphological changes in the lamellar structure, since no significant variations in the topography are observed. It is also interesting to note that, despite the persistent negative potential values acquired under high humidity conditions, the potential difference between each terrace surface and its neighboring step is constant and within a narrow range (60−100 mV), indicating that the negative charge is uniformly distributed throughout the crystal.

1. Introduction

Dewetting of liquid films form interesting patterns on the substrate, whose morphology depends on the liquid motions during dewetting and thus on the interactions among the various components of the system (substrate, solvent, and solutes).[1−3] Micro- and nanosized structures produced by this process are of great interest for the fabrication of microelectronic and optical devices and also for the understanding of the process evolution resulting in the final patterns.[4−6] Polymers receive special attention in this field due to their importance in many applications, and more recently, other long chain molecules, such as ionomers and surfactants have also be considered.[7−11]

We have shown in a recent work that a drop of SDS aqueous solution deposited on mica form characteristic patterns by drying and dewetting.[7] These are composed by branched structures topped by a flat surface and formed by steps and terraces with surfactant molecules organized in bilayers. Besides, images obtained by Kelvin force microscopy (KFM) revealed well-defined potential distributions on this sample, with marked differences between the steps and the terraces.

Modern techniques of microscopy, mainly scanning probe microscopy (SPM), are revealing interesting properties of solid surfaces, regarding the topography, and also electric, magnetic, hydrophilic, and other surface-related properties.[12−15] In the case of surfactants and other amphiphilic molecules, these studies are especially important because the self-organized structures formed by these molecules in liquid media are well-characterized, but little is known about their morphology after drying. Moeller et al.[16] used KFM to analyze assemblies of perfluoroalkyl alkanes spin-cast on mica, silicon, or graphite substrates. These molecules self-assemble into spirals, ribbons, and other structures, always presenting more negative electric potential than the substrates, under relative humidity (RH) within a 20−25% range. As the humidity is increased to 95% RH, the structures undergo significant changes in topography, with spiral assemblies changing into toroids, followed by changes in the electric potential values.

Microscopy techniques suitable for maping electric force (EFM) and electric potential (SEPM or KFM) adjacent to a surface have been used in this laboratory in the past years showing electric patterns more or less complicated on the surface of insulating solids.[17−24] Domains with both positive and negative charges coexist in neighboring areas, and the resulting patterns are very stable in some cases, while in others they respond to external stimuli, such as atmospheric relative humidity.

Particles of Stöber silica and aluminum phosphate were analyzed, as well as polymers, like polyethylene and different kinds of latex films. In the case of poly(styrene-*co*-hydroxyl methacrylate) (PS-HEMA) latex, films are shaped from spherical particles with core−shell ionic distribution. A comprehensive analysis by KFM and elemental imaging in transmission electrical microscopy (ESI-TEM) showed a close relationship between electric potentials measured at the surface and the distribution of potassium and sulfate ions, remaining from synthesis.[17,25]

In other cases, when the sample composition is not well-defined, charge carrier identification is more difficult. Formation and dissipation of electrostatic potentials on silica surface,[23,24] cellulose,[26] polyethylene,[21] metals,[27] and particles of Stöber silica[22] and aluminum phosphate,[22] under variable relative humidity conditions are consistent with a model based on the preferential adsorption of positive or negative water clusters on the surface. Atmospheric water is adsorbed and dissociates, forming $[H(H_2O)_n]^+$ or $[OH(H_2O)_n]^-$ ions that adsorb on the surface depending on the local prevailing potential and also on specific interactions. The formation and dissipation of electric potentials on these surfaces are thus dependent on the atmospheric humidity.

In the present work, characteristic electric potential patterns formed on SDS steplike samples are analyzed under variable relative humidity, under short (2 h) and long (24 h) times. Changes on the electric potential patterns measured using Kelvin

* Corresponding author, fernagal@iqm.unicamp.br.

10.1021/jp107291j
Published on Web 10/19/2010

force microscopy are observed as the relative humidity changes and the results are evaluated considering the selective water cluster adsorption model.

2. Experimental Methods

2.1. Sample Preparation and Analysis. Samples were prepared by placing 10 μL of a surfactant solution on freshly cleaved mica (Ted Pella), followed by drying at controlled relative humidity (50 ± 2%) and temperature (20 ± 2 °C). Surfactant solution was 2 mM sodium dodecyl sulfate (SDS) in Milli-Q water. SDS (99% pure) was purchased from Sigma and used without further treatment.

Dry samples were imaged by atomic force microscopy in electric potential (Kelvin) mode (KFM), yielding topography and electric potential maps simultaneously, from the same surface area. Images were obtained in a Shimadzu SPM 9600 microscope using a Pt-coated silicon nitride cantilever, with nominal resonance frequency of 82 ± 9 kHz and stiffness constant of 2.9 ± 0.3 N/m.

The microscope is fully contained within an environmental chamber that allows control of temperature, relative humidity, ambient pressure, and atmosphere composition. Pictures of the environmental chamber and its main parts are available as Supporting Information (Figure S1). Temperature was kept constant at 25 ± 2 °C during image acquisition, while relative humidity was varied in two series of experiments. In the first series, relative humidity was increased from 30 ± 2% to 50 ± 2% and then to 70 ± 2%, and images were acquired after keeping the sample for 2 h under each humidity. In the second experimental series, samples were maintained for 24 h in each humidity before imaging. The first image was obtained at 70 ± 2% and then the humidity was decreased to 50 ± 2% and 30 ± 2%.

2.2. Evaluation of the Surface Charge Density (σ). The distribution of excess charge on SDS dried on mica was evaluated using a procedure described previously.[7,21,24] This is based on comparison of the electric potential measured at any point close to the surface to the potential calculated applying the superposition principle to a virtual charge distribution.[28] The total electrostatic potential (V_T) generated by all surface charges at the plane 10 nm away from a charge-carrying surface (r = 10 nm) is thus calculated using a C^{++} code for eq 1

$$V_T = \sum_{i=1}^{n} V = \frac{1}{4\pi\varepsilon\varepsilon_0} \sum_{i=1}^{n} \frac{q_i}{r_i} \quad (1)$$

where q is the electric charge, ε_o is the permittivity of the free space, and ε is the dielectric constant of the medium.

A squared area (500 × 500 nm^2) of an electrostatic map obtained by KFM (indicated by the arrow in Figure 1d) is represented by a 12 × 12 pixel matrix. Four profiles are traced on the image and these are compared to potential profiles calculated for a virtual charge matrix of the same size created in MS Excel, carrying definite numbers of charges per pixel. The virtual charge distribution on the matrix is adjusted by trial and error, until the calculated and the experimental electric

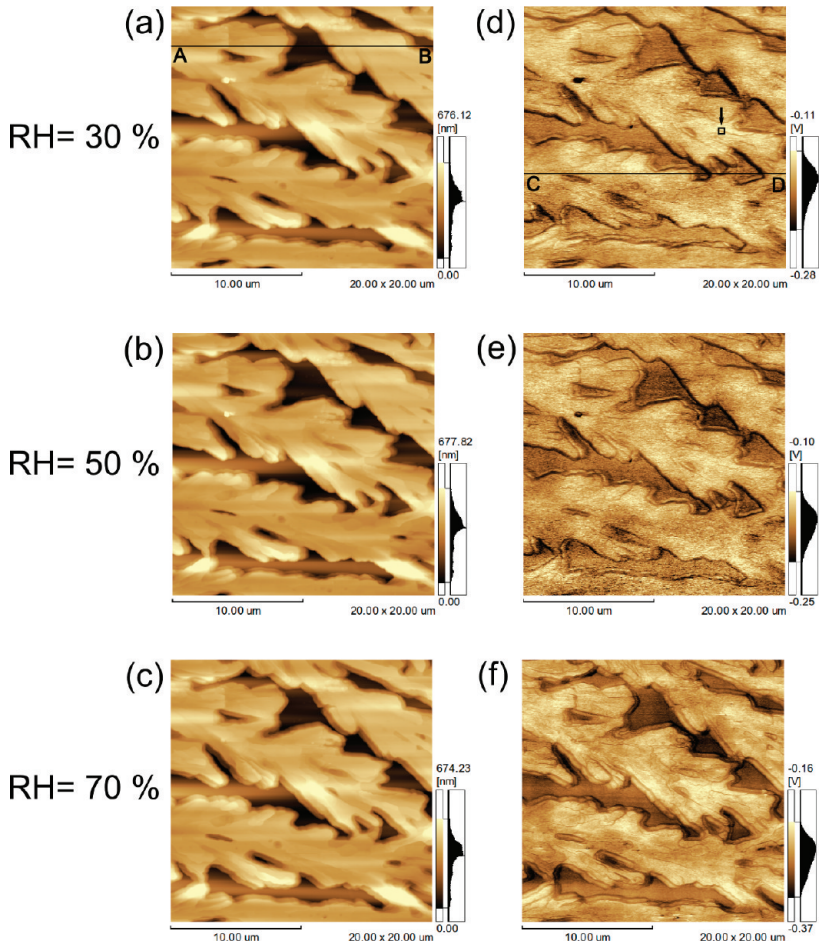

Figure 1. Topography (left) and KFM (right) images from SDS dried on mica, obtained at different relative humidities: (a, d) 30%, (b, e) 50%, and (c, f) 70%. Equilibrating time at each humidity was 2 h.

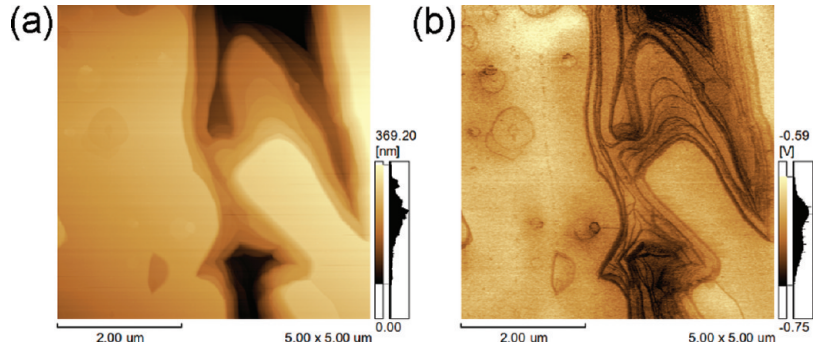

Figure 2. (a) Topography and (b) KFM image from SDS dried on mica, obtained at 50% RH. Equilibrating time was 8 h.

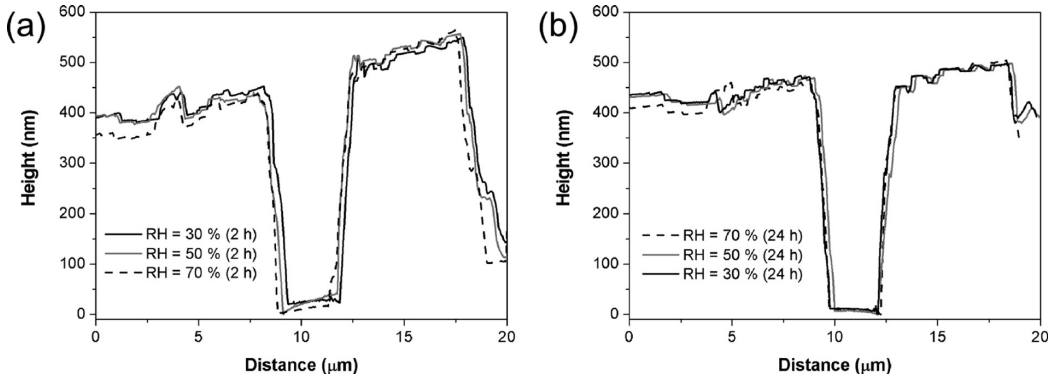

Figure 3. Height variations along a single line in SDS sample at different relative humidities and equilibrating times (line A−B, indicated in Figure 1a). Profiles were obtained from topography images in (a) Figure 1a−c, equilibrating time = 2 h, and (b) Figure 4a−c, equilibrating time = 24 h.

potentials have a similar profile. The surface charge excess was obtained within this 0.25 μm^2 area.

3. Results

Dewetting of diluted SDS solutions on mica surface forms long branched stripes, as a result of fingering instability. Within dewetting morphology, surfactant molecules are packed in a lamellar structure, forming flat and uniform layers that are observed by AFM and KFM.[7] In the present work, potential distribution along the SDS layered structure was analyzed while changing relative humidity within an electrically shielded and grounded environment.

Topography and Kelvin micrographs obtained after step changes in relative humidity are presented in Figure 1. Images were acquired after the sample was left for 2 h to reach equilibrium at 30%, 50%, and 70% RH. This sequence of images will be referred to as "first series", throughout text.

These images show the characteristic pattern formed by the SDS sample under these drying conditions: a fingering morphology formed by layers of surfactant molecules. The surfactant layered structure is more clearly demonstrated in Figure 2a, and this pattern is very stable concerning both the surfactant packing and the pattern dimensions under variable relative humidity conditions.

Height distribution histograms in Figure 1a−c and topography line profiles presented in Figure 3a show only minor differences as the relative humidity rises, indicating that water sorption does not promote noticeable swelling of this sample under the experimental conditions used. These profiles were obtained from AFM images presented in Figure 1a−c in the same line A−B (indicated in Figure 1a). Topography profiles obtained for SDS sample kept for 2 h at relative humidities from 30 to 70% RH (Figure 3a) are very similar, with maximum height reaching 400−550 nm.

The corresponding Kelvin measurements show that electric potential is negative at any sample point (Figures 1d−f and 2b). Potential histograms in parts d and e of Figure 1 (for samples at 30% and 50% RH, respectively) cover the same potential range, showing that the electric potential distributions are very similar under these two humidity conditions. However, as the relative humidity increases from 50% to 70% RH, the average potential becomes more negative (Figure 1f). The higher water content in the atmosphere thus leads to an increase in the overall sample charge even within the shielded and grounded microscope sample environment. The electric contrast highlights the surfactant layered structure: steps between surfactant layers are more negative than the layer surface terraces. This can be more clearly observed in Figure 2b for an SDS sample imaged after 8 h at 50% RH.

Slow potential changes are observed in another sequence of images (second series), shown in Figure 4. Topography and the corresponding electric potential images were sequentially acquired at 70%, 50%, and 30% RH in the same sample area shown in Figure 1, but now allowing the sample to stay for 24 h under each relative humidity before image acquisition.

Topography images (Figures 4a−c) show the same fingering morphology with layered SDS structures deposited on mica. Height histograms also concentrate in the same region shown in Figure 1 (from 70 to 380 nm) and the topographic profiles obtained in line A−B at different relative humidities (Figure 3b) are well superposed. These results show that even longer exposure to water vapor does not promote significant changes in film morphology and thickness.

Considering the potential behavior, the Kelvin micrographs (Figure 4d−f) show negative electric potential throughout, but the electric potential values in these figures are much lower than the values obtained in Figure 1, under shorter exposure to water vapor. The continuous decrease in electric potential as the

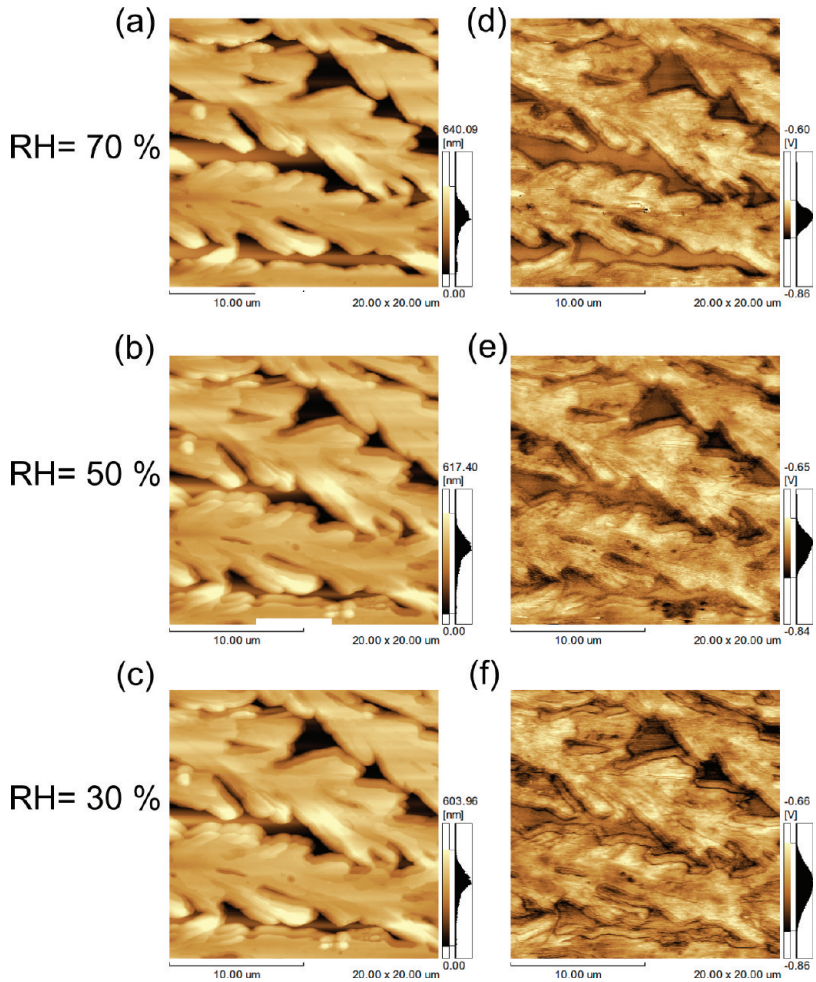

Figure 4. Topography (left) and KFM (right) images from SDS dried on mica, obtained at different relative humidities: (a, d) 70%, (b, e) 50%, and (c, f) 30%. Equilibrating time at each humidity was 24 h.

sample is kept at a certain humidity shows that the potential changes are slow and that the electrification of the samples is strongly dependent on its kinetics.

Potentials can be better evaluated by comparing line profiles traced along the same line in Figures 1 and 4, with different exposure times at 30%, 50%, and 70% RH. The analyzed line (C−D) is drawn in Figure 1d and the potential profiles are presented in Figure 5. Profiles obtained after 2 h present less negative potential than samples exposed to a humid environment for 24 h. These results confirm the kinetic factor mentioned above, showing that under relatively long exposure times, samples acquire more negative potentials, due to an increase in the excess negative charge at the surface.

Another important aspect shown by the potential profiles is that the acquired charges do not dissipate fast under low humidity. Following the order of experiments in Figure 5, it is possible to verify that potentials remain unchanged (around −0.15 V) in samples kept for 2 h under 30% or 50% RH and then decrease to ca. −0.25 V when the humidity increases to 70%. Then samples are left for 24 h at 70% RH and the potentials decrease even more to around −0.7 to −0.8 V. Finally, when the humidity is increase again to 50% or 30%, potentials are not dissipated, indicating that irreversible changes take place in the sample, as it is cycled through dry and humid environments.

Potential gradients can be calculated at any position in the sample from the line scans in Figure 5. This yields the field

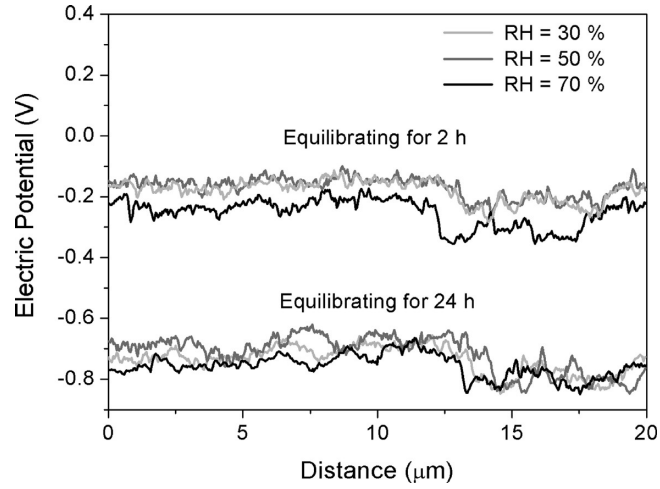

Figure 5. Electric potential variations along a single line in SDS sample at different relative humidities and equilibrating times. Profiles were obtained from KFM images in Figures 1d−f and 4d−f in the region exemplified by the line C−D in Figure 1d.

component along the *x* axis. Potential gradients obtained at different experimental conditions are shown in Figure 6 and reveal that SDS deposited on mica presents significant electric fields varying from −0.8 to +0.8 MV/m. Moreover, the gradient curve for the sample under 30% RH (initial condition) is

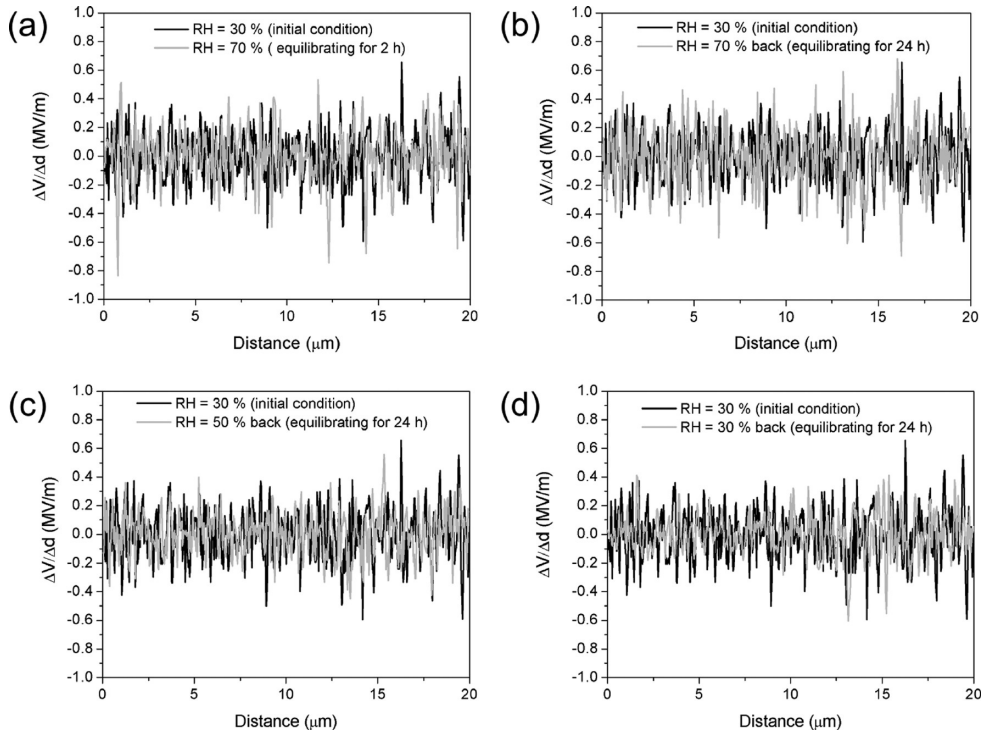

Figure 6. Electric potential gradients calculated as a function of distance from SDS sample at the initial condition (30% RH after 2 h, solid line in all plots) and at (a) 70% RH after 2 h, (b) 70% RH after 24 h, (c) 50% RH after 24 h, and (d) 30% RH after 24 h.

practically identical, when compared to the curves under higher relative humidity, indicating that SDS surface acquires charge uniformly, without enhancing or smoothing local electric gradients.

Step−Surface Analysis. To analyze the potential variation between the step and the surface in SDS lamellae, a squared area (500 × 500 nm^2) was digitally magnified in all the electrostatic maps from Figures 1d−f and 3d−f. The same area is considered in all the images and is shown in Figure 7. The black squared area in Figure 1d shows the magnified region.

It is remarkable that although the sample acquires a persistent negative electric potential under exposure to higher humidity, the potential difference between the terrace surface and the neighboring step is within a narrow range (from −60 to −100 mV), in all cases, as shown in the histograms from Figure 7a−f. This potential difference is observed in many steps analyzed in the samples, imaged under all the humidity values used.

Electric potential profiles can be obtained from images in Figure 7 and compared to electric potential profiles calculated using the superposition principle of electrostatics. As described in the experimental procedure, a simulation is carried out to find a virtual distribution of charges that results in a specific potential distribution on the image. Measured and simulated potentials are compared through profiles traced along four lines on the image and on the matrix. The virtual charge distribution that coincides simultaneously with the four experimental profiles in each area is taken as the representative charge excess distribution for this area. Examples showing the comparison between three experimental potential curves (obtained from the same line E−F in panels a, c, and d of Figure 7) and the respective calculated profiles are shown in Figure 8. Reasonable agreement is observed between the curves.

The simulated surface charge excess obtained for all the images presented in Figure 7 are plotted in Figure 9. In the initial condition (30% RH), the sample presents ca. 15 negative charges in excess, within this 500 × 500 nm^2 area. As the relative humidity is increased to 70%, the charge excess increases ca. 65% (to 22 negative charges). When the samples are maintained for 24 h at 70% RH, the charge excess increases up to ca. 90, staying at this level. The surface charge density values at different relative humidities are listed in Table 1.

4. Discussion

An SDS aqueous solution deposited on mica and dried under the experimental conditions used in this paper forms organized patterns due to simultaneous drying and dewetting. SDS branched patterns are made up of steps with SDS molecules placed side by side and oriented perpendicularly to the mica surface, as discussed in a previous publication.[7] This results in a structure with well-defined potential differences between the steps and the layer surfaces, since the first is mainly formed by polar headgroups, and the second by hydrophobic chains.

Dimension changes in any direction are not detected in topography images (Figures 1 and 4) or profiles (Figure 3) as the relative humidity increases. Anisotropic swelling would be expected under wet conditions, as observed by other authors,[29,30] due to water sorption into the hydrophilic sites of the surfactant lamellae. Fontell et al.[30] showed that the aqueous channels in a lamellar phase can swell ca. 7 nm when the total water content in the system increases from 25% to 80% wt. However, in the case of the dry SDS lamellar phase exposed to a humid environment, swelling is not experimentally detected.

The overall potential observed on the samples is very similar, after 2 h exposure to 30% and 50% RH, but becomes more negative, as the humidity is increased to 70%, as shown in Figures 1 and 5. The only parameter changed here is the atmospheric water content. The chamber is grounded and the samples are protected from charging by contact, induction, triboelectrization, or charge injection. Following the work hypothesis used in previous works, charge carriers are water clusters containing hydronium $[H(H_2O)_n]^+$ and hydroxide ions

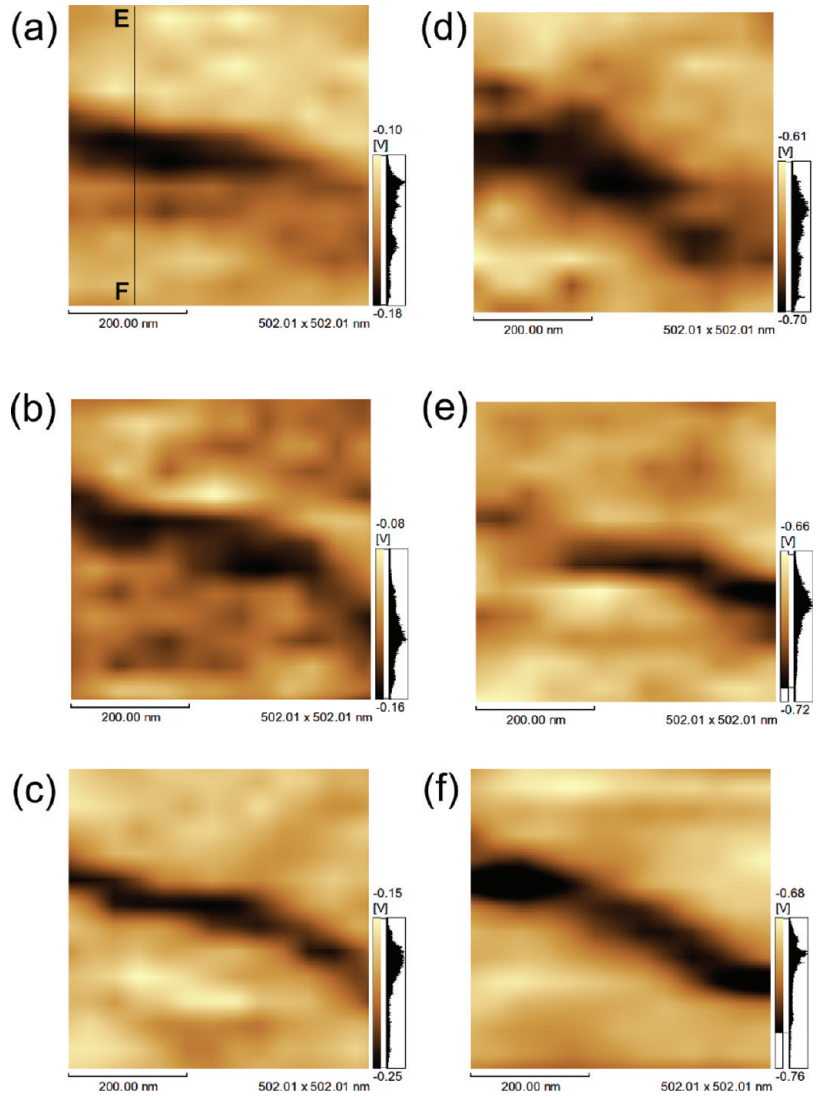

Figure 7. Amplified region of the KFM images obtained at (a) 30% RH after 2 h, (b) 50% RH after 2 h, (c) 70% RH after 2 h, (d) 70% RH after 24 h, (e) 50% RH after 24 h, and (f) 30% RH after 24 h. The zoomed area is indicated by the arrow in Figure 1d.

$[OH(H_2O)_n]^-$ exchanged with the surface through water vapor adsorption and desorption. The accumulation of excess negative charges on an SDS surface is then assigned to selective adsorption of hydroxide groups from atmospheric water.

These results parallel with the well-established selective OH^- adsorption[31−35] at hydrophobic interfaces, such as oil/water. The free energy of this specific interaction was estimated to be very pronounced (ca. 20 kT per ion).[35] Mariova et al.[32] proposed that the reason for this preferential adsorption is the strong hydrogen bonding established between OH^- ions and water molecules adsorbed at the interface, compared to those formed with water molecules in the liquid bulk, revealing that the water at the interface is much stronger acid than bulk water.[31] The same argument is now applied to OH^- ion binding to water adsorbed on SDS surfaces, as compared to its bonding to water clusters in the gas phase.

The charge excess on an SDS surface, after cycling the sample through high and lower humidity, corresponds to one hydroxide ion for every 2700 nm^2, which is much lower than the value measured at the oil/water interface under ionic strength in the mmol L^{-1} range (one hydroxide ion per 3 nm^2).[33] This relevant difference in charge excess is due to OH^- abundance in the continuous medium. In the present case of SDS/mica system under a gas phase, the continuous medium for charge carriers is the water vapor, which contains much lower density of water molecules in number.

Many experimental results previously obtained by this group[21−24,26] have already been understood following this simple electrification model, where the atmosphere acts as a reservoir of charges for dielectrics. For instance, films of noncrystalline silica and aluminum phosphate particles closed within an electrically shielded and grounded environment had their potentials altered just by changing the atmospheric humidity and thus the ions absorption/desorption ratio.[22] Silica surface became more negative at higher humidity, while aluminum phosphate became more positive.

The irreversibility of the charging/discharging cycle and the remaining excess of negative charges on the solid surface after a long exposure time to high humidity must be related to the energy gain involved in the bonding between the negative water cluster $[OH(H_2O)_n]^-$ and the oriented water layer on the hydrophobic surface (ca. 20 kT per ion). This favorable interaction makes the process very slow or even irreversible within the experimental conditions used.

Irreversibility of surface potentials measured by KFM when cycling the samples through high and low humidity was also observed on aluminum phosphate particle films but not on silica particle surfaces.[22] In the second case, potential values initially

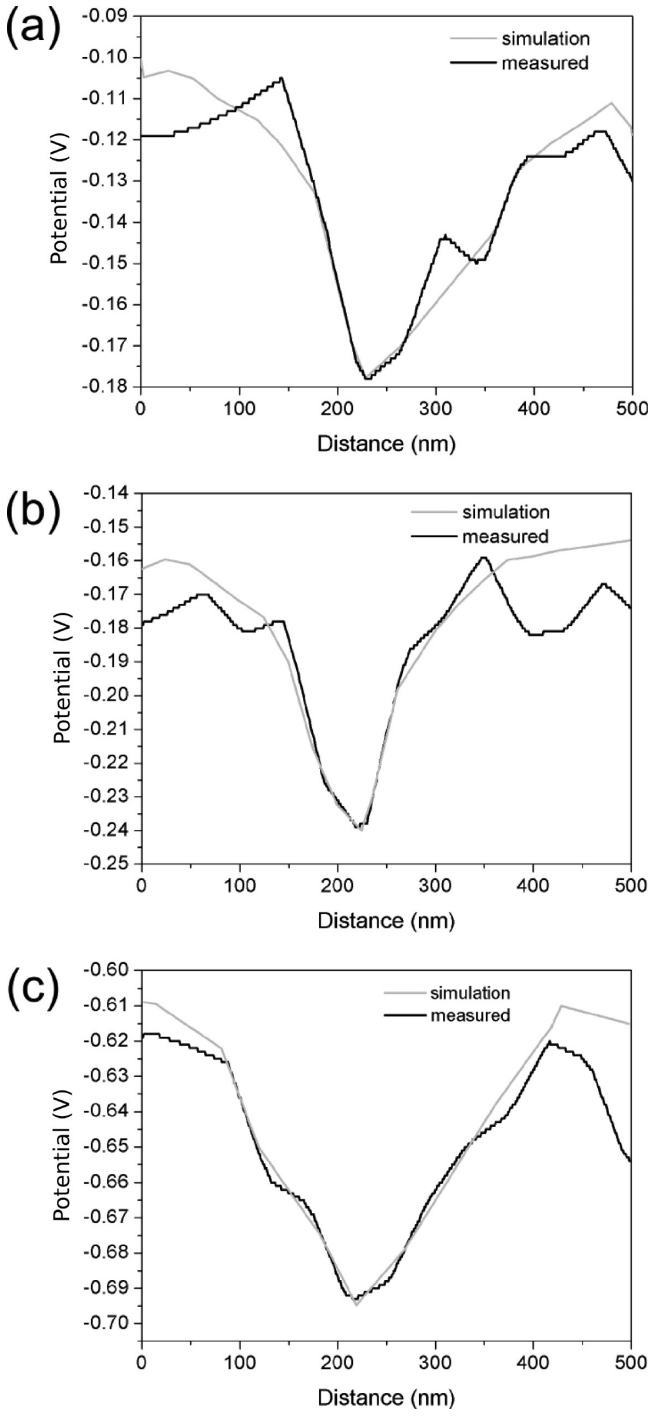

Figure 8. Calculated and experimental electric potential profiles in SDS sample for line E−F indicated in Figure 7a: (a) 30% RH after 2 h; (b) 70% RH after 2 h; (c) 70% RH after 24 h.

obtained at 30% RH are recovered after submitting the sample to 70% and then to 30% RH again.

SDS surface acquires charges homogeneously by changing humidity, resulting in a constant potential difference (60−100 mV) between the step and the terrace surface, as shown in Figure 7. Moreover, surface potential gradients along an SDS sample are smaller than those found on aluminum phosphate and silica.[22] Aluminum phosphate shows gradient spikes in excess of ±4MV/m, while in the SDS case, gradients reach extremes of ±0.8 MV/m (as shown in Figure 6). This difference can be related to the solid structure. SDS has a crystalline structure, with surfactant molecules oriented in flat and uniform layers. Water

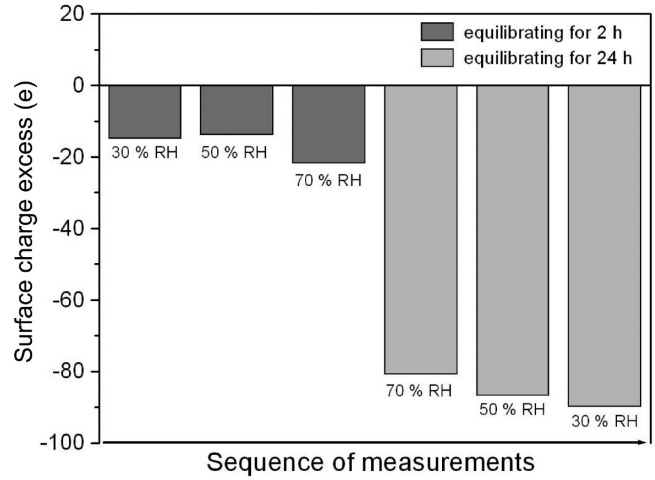

Figure 9. Surface charge excess (e) for SDS sample at different experimental conditions.

TABLE 1: Surface Charge Density at Different Relative Humidities

relative humidity	surface charge density $\times 10^{-6}$ (C/m^2)
30% RH (2 h)	10
50% RH (2 h)	9
70% RH (2 h)	14
70% RH (24 h)	51
50% RH (24 h)	55
30% RH (24 h)	57

molecule adsorption on the uniform SDS terraces should be spatially uniform, creating uniform sites for $[OH(H_2O)_n]^-$ location. Moreover, charge delocalization on water adsorbed layers or clusters should be very intense, according to Grotthuss charge transfer mechanism.[36] This is quite different from silica and aluminum phosphate particles that are nonequilibrium ionic structures with large intrinsic potential gradients.

5. Conclusions

Electrostatic potential measured along the SDS surface changes with relative humidity, within a grounded environment. This is interpreted assuming that hydroxide ions, released from water molecules, adsorb preferentially at the vapor−solid interface. The selective and hysteretic $[OH(H_2O)_n]^-$ adsorption is related to the strong hydrogen bonding established between the negative ions and the oriented water layer adsorbed on the surfactant surface. Negative charge acquisition is uniform along SDS surfaces due to Grotthus charge delocalization.

Acknowledgment. FAPESP (São Paulo) is acknowledged for the financial support to this work and for postdoctoral scholarships to J.S.B and C.A.R.. This is a contribution from the INCT Inomat—National Institute for Science and Technology of Complex Functional Materials (MCT-FAPESP).

Supporting Information Available: 1. Pictures of the AFM environmental chamber showing its main parts. This material is available free of charge via the Internet at http://pubs.acs.org.

References and Notes

(1) Sharma, A.; Reiter, G. *J. Colloid Interface Sci.* **1996**, *178*, 383.
(2) Seemann, R.; Herminghaus, S.; Jacobs, K. *Phys. Rev. Lett.* **2001**, *86*, 5534.
(3) Lee, L. T.; da Silva, M. C. V.; Galembeck, F. *Langmuir* **2003**, *19*, 6717.

(4) Huwiler, C.; Halter, M.; Rezwan, K.; Falconnet, D.; Textor, M.; Voros, J. *Nanotechnology* **2005**, *16*, 3045.
(5) Rezende, C. A.; Lee, L. T.; Galembeck, F. *Langmuir* **2007**, *23*, 2824.
(6) Luo, C.; Xing, R.; Zhang, Z.; Fu, J.; Han, Y. *J. Colloid Interface Sci.* **2004**, *269*, 158.
(7) Bernardes, J. S.; Rezende, C. A.; Galembeck, F. *Langmuir* **2010**, *26*, 7824.
(8) Carvalho, A. J. F.; Pereira-da-Silva, M. A.; Faria, R. M. *Eur. Phys. J. E* **2006**, *20*, 309.
(9) Afsar-Siddiqui, A. B.; Luckham, P. F.; Matar, O. K. *Langmuir* **2004**, *20*, 7575.
(10) Cachile, M.; Schneemilch, M.; Hamraoui, A.; Cazabat, A. M. *Adv. Colloid Interface Sci.* **2002**, *96*, 59.
(11) Qu, D.; Suter, R.; Garoff, S. *Langmuir* **2002**, *18*, 1649.
(12) Meincken, M.; Klash, A.; Seboa, S.; Sanderson, R. D. *Appl. Surf. Sci.* **2006**, *253*, 805.
(13) Rezende, C. A.; Lee, L. T.; Galembeck, F. *Langmuir* **2009**, *25*, 9938.
(14) Ye, Z.; Zhao, X. *J. Microsc.* **2010**, *238*, 27.
(15) Sugimura, H.; Hayashi, K.; Saito, N.; Nakagiri, N.; Takai, O. *Appl. Surf. Sci.* **2002**, *188*, 403.
(16) Alexander, J.; Magonov, S.; Moeller, M. *J. Vac. Sci. Technol., B* **2009**, *27*, 903.
(17) Cardoso, A. H.; Leite, C. A. P.; Galembeck, F. *Langmuir* **1998**, *14*, 3187.
(18) Braga, M.; Costa, C. A. R.; Leite, C. A. P.; Galembeck, F. *J. Phys. Chem. B* **2001**, *105*, 3005.
(19) Santos, J. P.; Corpart, P.; Wong, K.; Galembeck, F. *Langmuir* **2004**, *20*, 10576.
(20) Costa, C. A. R.; Leite, C. A. P.; Souza, E. F.; Galembeck, F. *Langmuir* **2001**, *17*, 189.
(21) Rezende, C. A.; Gouveia, R. F.; Silva, M. A.; Galembeck, F. *J. Phys.: Condens. Matter* **2009**, *21*, 263002.
(22) Gouveia, R. F.; Galembeck, F. *J. Am. Chem. Soc.* **2009**, *131*, 11381.
(23) Gouveia, R. F.; Costa, C. A. R.; Galembeck, F. *J. Phys. Chem. B* **2005**, *109*, 4631.
(24) Gouveia, R. F.; Costa, C. A. R.; Galembeck, F. *J. Phys. Chem. C* **2008**, *112*, 17193.
(25) Cardoso, A. H.; Leite, C. A. P.; Galembeck, F. *Langmuir* **1999**, *15*, 4447.
(26) Soares, L. C.; Bertazzo, S.; Burgo, T. A. L.; Baldim, V.; Galembeck, F. *J. Braz. Chem. Soc.* **2008**, *19*, 277.
(27) Ducati, T. R. D.; Simões, L. H.; Galembeck, F. *Langmuir* **2010**, *26*, 13763.
(28) Griffiths, D. J. *Introduction to Electrodynamics*, 3rd ed.; Prentice Hall: Upper Saddle River, NJ, 1999; p 60.
(29) Bernardes, J. S.; Norrman, J.; Piculell, L.; Loh, W. *J. Phys. Chem. B* **2006**, *110*, 23433.
(30) Fontell, K.; Khan, A.; Lindström, B.; Maciejewska, D.; Puang-Ngern, S. *Colloid Polym. Sci.* **1991**, *269*, 727.
(31) Healy, T. W.; Fuerstenau, D. W. *J. Colloid Interface Sci.* **2007**, *309*, 183.
(32) Marinova, K. G.; Alargova, R. G.; Denkov, N. D.; Velev, O. D.; Petsev, D. N.; Ivanov, I. B.; Borwankar, R. P. *Langmuir* **1996**, *12*, 2045.
(33) Beattie, J. K.; Djerdjev, A. N.; Warr, G. G. *Faraday Discuss.* **2009**, *141*, 31.
(34) Kudin, K. N.; Car, R. *J. Am. Chem. Soc.* **2008**, *130*, 3915.
(35) Gray-Weale, A.; Beattie, J. K. *Phys. Chem. Chem. Phys.* **2009**, *11*, 10994.
(36) Atkins, P. W. *Physical Chemistry*, 5th ed.; Oxford Press: Oxford, 1994; p 840.

JP107291J